Molecular motor organization and mobility on cargos can overcome a tradeoff between fast binding and run length

Matthew Bovyn[a,1], **Steven Gross**[b,a,c,1], **Jun Allard**[a,d,1,*]

***For correspondence:** jun.allard@uci.edu (JA)

[a]Department of Physics and Astronomy, University of California, Irvine; [b]Department of Developmental and Cell Biology, University of California, Irvine; [c]Department of Biomedical Engineering, University of California, Irvine; [d]Department of Mathematics, University of California, Irvine; [1]Center for Complex Biological Systems, University of California, Irvine

Abstract Eukaryotic cells transport cargos, including organelles like lipid droplets and mitochondria, along microtubule tracks using molecular motors. Different cargo are in some cases routed to different subcellular locations, which is essential for organization of the cell interior in space and time. While a great deal is known about the single molecule properties of motors, it is still unclear how the cell coordinates these motors to achieve cargo-specific transport outcomes. One possible mode of regulation is through the organization and mobility of motors on the surface of the cargo. In this work we use physics-based 3D mathematical modeling to investigate how cargos are transported under different assumptions of motor anchoring. We compare cases where motors are free to diffuse in the cargo membrane to cases where motors are rigidly anchored to the cargo with different distributions. We find that different modes of anchoring give rise to differences in transport properties, such as cargo binding rate to the microtubule, run lengths, and forces generated. Cargos with clustered motors are transported efficiently, but are slow to bind to a nearby microtubule. Cargos with motors dispersed rigidly on their surface bind the microtubule quickly, but are not transported efficiently. Cargos with freely-diffusing motors bind the microtubule quickly, and are transported more efficiently than the rigid-dispersed arrangement, although not as efficiently as the clustered arrangement. These results point to a functional role for recently observed changes in motor organization on cargos in the cell. They also suggest motor diffusivity as a control point the cell may use to differentially transport types of cargos, either by using adaptor proteins with different membrane anchors or by controlling lipid composition of the cargo membranes.

Introduction

To organize their internal structure, eukaryotic cells employ molecular motors in the kinesin and dynein superfamilies to transport organelles and other cargo along microtubules. Despite having only a limited set of cargo transport motors (kinesin-1, kinesin-2 and kinesin-3 families (***Verhey et al., 2011***), along with cytoplasmic dynein), different cargos are transported to different locations, even though they are transported along the same set of microtubule "roads". For example, under normal conditions COS-7 cells direct lipid droplets toward microtubule plus ends, localizing them

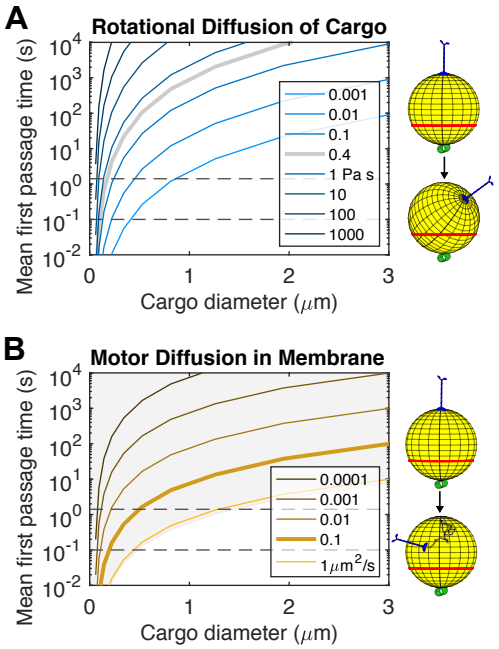

Figure 1. Mean first passage times (MFPTs) for a motor initially located opposite the microtubule to come within binding range by:
A: rotational diffusion of the cargo. Shown for various values of viscosity of the surrounding fluid. Values are chosen to span the range of values estimated for cytoplasm (***Yamada et al., 2000***). Grey curve is at viscosity 0.4 Pa s, measured in ***Wilhelm et al.*** (***2003***).
B: diffusion of the motor in the cargo surface. Shown at various values of the diffusion coefficient. MFPTs for diffusion coefficients achievable when the surrounding fluid has viscosity of 0.4 Pa s are shaded in grey (***Saffman and Delbrück, 1975***).
For details on calculation, see figure ***Figure 1–Figure Supplement 1***.

Figure 1–Figure supplement 1. Mean reach elevation

near the plasma membrane, and mitochondria toward the minus end, localizing them near the nucleus. Under glucose starvation, localization of both organelles changes to spread them out around the cell, allowing them to come into contact with each other (***Herms et al., 2015***). How do cells achieve these cargo-specific routing outcomes? In some cases, cells use molecular specificity to achieve cargo specificity, such as using specific linkers or cargo-bound regulators (***Maday et al., 2014***; ***Akhmanova and Hammer, 2010***).

In this paper, we seek to model modes of transport regulation that are not based on biochemical specificity, but rather, on physical properties of the cargo. For example, cargo size, and where and how motors are attached to the surface of the cargo, may contribute to routing. Recent experiments raise both these possibilities. In J774 macrophages, larger phagosomes are transported directly toward the nucleus while smaller ones spend more time moving bi-directionally (***Keller et al., 2017***). In *Dictyostelium*, dynein organization on the cargo surface changes from spread out to clustered as phagosomes mature (***Rai et al., 2016***). Past work using computational modeling has called attention to motor organization as a regulator of transport (***Erickson et al., 2011***). Here we expand on that work by considering a mode of motor organization on cargos which is so far little explored — motors which are free to diffuse in the cargo membrane.

Many cellular cargos are encased in membranes, raising the possibility that motors diffuse in that membrane. Freedom of motors on the surface of cargos has been of recent experimental interest and several papers have compared the collective action of kinesin motors which are free to diffuse in membranes to cases where they are rigidly attached to a surface, both in the microtubule gliding assay configuration (***Grover et al., 2016***) and the bead assay configuration (***Li et al., 2018***). These studies show that motor freedom in membranes can influence transport properties, but it is

unclear how to translate the *in vitro* results into the context of the cell, especially since the studies have contradictory results (transport is slowed in the gliding assay vs. sped up in the bead assay). Furthermore, Li et al. find that the increase in velocity is small with no difference in how far cargos travel overall. This confounds the impact which freedom to diffuse may have on cargo transport in the cell.

To gain intuition for how the above experiments, which were performed *in vitro*, may be extrapolated into the cellular environment, we perform a simple calculation. We ask how long it would take for a motor initially located opposite the microtubule to come within range of the microtubule to bind to it, under two different assumptions of how that motor is able to move: first by rotational diffusion of the cargo body moving a rigidly bound motor, and second by diffusion of a motor in the membrane of a non-moving cargo (illustrated in the diagrams accompanying figure 1 A and B respectively). By examining figure 1, we find that for any choice of cargo size, the time it takes for a motor to come near enough to the microtubule to bind is similar for cargo rotational diffusion at the viscosity of water (~ 0.001 Pa s) and for surface diffusion at the diffusion coefficient of motors in the *in vitro* supported lipid bilayers used in the experiments mentioned above ($\sim 1\ \mu m^2\ s^{-1}$). For the less than 1 µm diameter cargos used in bead assays, both these modes have times which fall in the range of characteristic times proposed for motor binding ((***Xu et al., 2012***; ***Feng et al., 2018***; ***Bergman et al., 2018***)). However, cargos in the cell have been repeatedly measured to diffuse less freely than in water. While a wide range of viscosity values has been inferred from these measurements (***Yamada et al., 2000***), the most similar measurement we know of to the specific case of a ~ 1 µm cargo rotating was made by Wilhelm and colleagues (***Wilhelm et al., 2003***). They find a viscosity of 0.4 Pa s, several hundred times greater than water (figure 1A, thick grey line) and similar to the viscosity used in (***Chowdary et al., 2018***). At this viscosity, rotational diffusion times are several orders of magnitude slower than in water. Importantly, they are also several orders of magnitude slower than diffusion of motors at typical values of diffusion coefficients for cellular transmembrane proteins (figure 1B, thick line, BioNumbers BNID:114189 (***Milo et al., 2010***)). For more details on this calculation, see ***Figure 1–Figure Supplement 1***.

The drastic differences in the time it takes for a motor to enter binding range of the microtubule between rotational diffusion of the cargo and the translational diffusion of a motor in the cargo membrane evoke the possibility that the time for a cargo to bind to a nearby microtubule in the cell could be drastically changed by the freedom of motors to diffuse. The subsequent transport of a cargo also depends strongly on the number of motors that are able to access the microtubule (***Erickson et al., 2011***). Therefore, motor freedom also has the potential to change other important transport properties such as run length and force generation.

The calculation plotted in figure 1 is highly simplified: it ignores binding times, motor on rates, and does not tell us about subsequent transport. Furthermore, cellular cargos are often moved by several motors simultaneously (***Shubeita et al., 2008***). Here we construct a computational model of cargo transport which includes multiple motors which are able to diffuse in the cargo membrane. Our model builds on a rich history of theoretical work on motors including analytical (***Klumpp and Lipowsky, 2005***), as well as computational (***Kunwar et al., 2008***) models. Several recent models including the diffusion of motors (***Lombardo et al., 2017***; ***Chowdary et al., 2018***) have been successful in helping to understand experimental data in specific configurations of cargo, motors and filaments. These models were derived using simplifying assumptions about membrane fluidity and surface flows, which when treated generally are computationally difficult and result in nontrivial fluid effects (***Sigurdsson and Atzberger, 2016***). In this paper, we seek to take a more comprehensive look at how cargos with different motor organizations are transported, and how transport outcomes change with physical properties of the cargo. To do so, we compare transport properties over a wide range of membrane fluidities, from fluid to solid. We then use this model to investigate transport outcomes of cargos with motors organized in different arrangements and mobilities, with a focus on the less-explored case of cargos which have motors which are free to diffuse in the membrane.

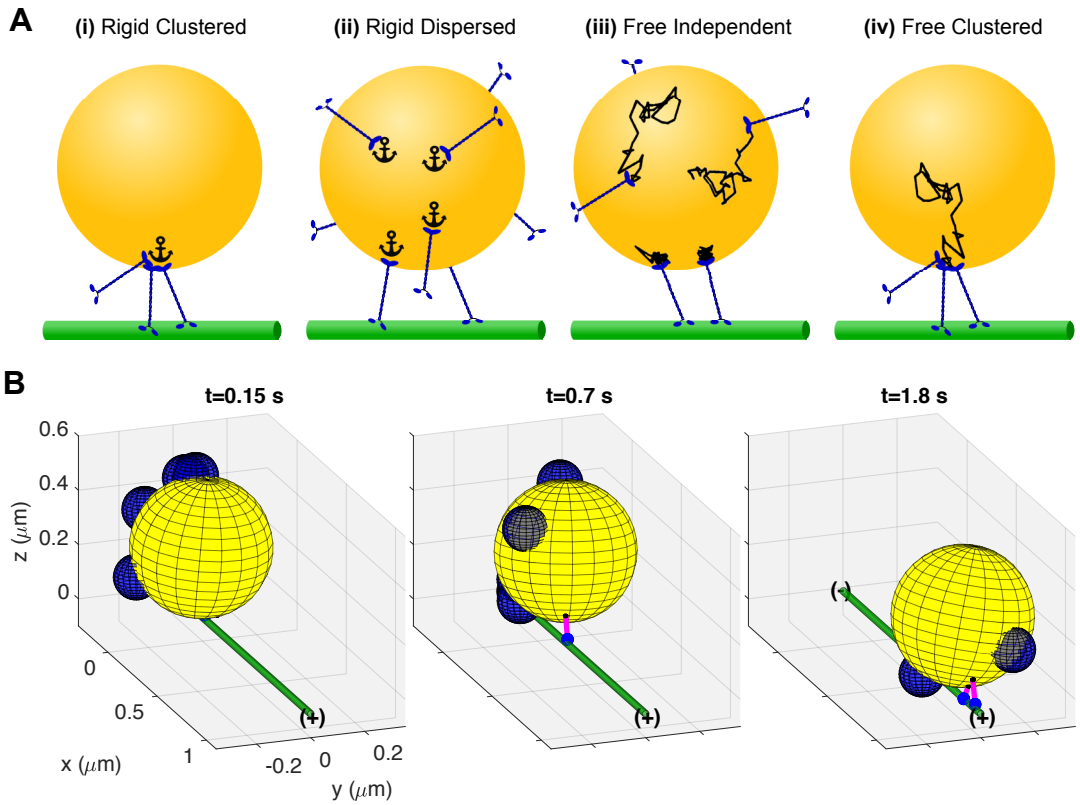

Figure 2. Motor organization modes and simulation snapshots.
A: Motors anchoring modes to be investigated. Cargo shown in yellow, motors in blue and microtubule in green. We name the states: rigid clustered (**i**), rigid dispersed (**ii**), free independent (**iii**), and free clustered (**iv**).
B: Series of simulation snapshots. The cargo is in yellow and the microtubule in green. The blue hemispheres represent the reach length of unbound motors, which have their anchor point at the center of the hemisphere. Bound motors are represented with a magenta stalk, small black anchor point and larger blue sphere at the center of mass location of the motor heads.

Figure 2–video 1. Animation from example simulation of cargo with free independent motors in 2B

Results

A computational model of cargo transport including freedom of motors to diffuse in the cargo membrane

We wish to explore the impact of surface organization of motors on specific transport outcomes. Because there are an infinite number of ways to arrange motors on a cargo, we narrow our scope to a few specific cases. We choose four extreme cases, as shown in figure 2A, which we term organization modes. The first two modes have motors bound rigidly to the cargo. They differ in how motors are spaced; the first mode we term “rigid clustered" places all the motor anchors at the same point, while in the second mode, which we term “rigid dispersed", the motor locations are random, drawn from a uniform distribution over the surface. The other two modes have motors which are free to diffuse in the cargo surface. In the “free independent" mode, the motor anchors do not interact with each other, other than through forces they exert on the cargo. In the final mode, termed “free clustered", all motor anchors are bound together, but the ensemble is able to diffuse in the cargo membrane. In this mode, we assume the cluster of motors diffuses with a reduced diffusion coefficient so that $D \sim 1/\sqrt{N}$ where N is the number of motors, which is consistent with motors being arranged in roughly a disk (***Saffman and Delbrück, 1975***) (rather than, e.g., in a row).

To investigate transport outcomes of cargos in these four different organization modes, we construct a three dimensional model of a cargo, the motors, and a microtubule. We model the cargo

as an undeformable sphere. We attach motors to the cargo at points which we term the anchors. We model these motors using the well studied chemomechanics of kinesin-1. These motors can bind the microtubule when the anchor is within reach of the microtubule (blue hemispheres in figure 2B represent motor reach length). Once bound, they step along the microtubule and unbind from it with rates that have been intensely studies *in vitro*. We draw our chemomechnical model for kinesin from recent experimental (***Andreasson et al., 2015***) and modeling (***Sumi, 2017***) efforts. For more details, see supplement sections A.1.1 and A.3.

As motors step, they exert forces on the cargo which would both tend to pull the cargo along through the surrounding fluid, and drag the anchor through the cargo membrane. In our model, forces which would drag the anchor through the cargo membrane result both in displacement of the anchor in the membrane and rotation of the cargo, in proportion to the anchor diffusion coefficient. Forces acting to move the cargo body do so against viscous drag, as we model the surrounding fluid as Newtonian. While recent measurements suggest the cytoplasm is an actively-driven, complex fluid with significant elasticity (***Guo et al., 2014***; ***Ahmed et al., 2018***), methods for simulating diffusion and the effect of further active forces in this environment are still in development. Modeling the cytoplasm surrounding the cargo as Newtonian allows us to qualitatively capture that some cargos in cells may be relatively free to move, while others may be significantly impeded by their local environment.

Both cargo and motors diffuse in their respective (3D or 2D) fluids. The cargo diffuses both rotationally and translationally with statistics governed by the Fluctuation-Dissipation Theorem, as implied by the viscosity of the surrounding fluid. Motors diffuse in the cargo surface with statistics governed by a diffusion coefficient. In general, complex movement may result from the interaction of motor anchors with different lipid domains (***Rai et al., 2016***) or other structures (for example, diffusion of cell surface proteins is influenced by the underlying actin cortex (***Kusumi et al., 2014***)).

A full description of the model and derivation of the equations we simulate can be found in supplemental section A. Details on the simulation can be found in supplemental section B and parameter values listed in table A1 are used for all simulations, unless otherwise indicated.

To obtain transport properties of cargos in different organization modes, we simulate 100 or more stochastic trajectories and examine the resulting distributions. We simulate trajectories using a hybrid Euler-Maruyama-Gillespie scheme, and report a series of tests which show that the code reproduces expected results in some simplified situations in supplemental section C. Snapshots from a single trajectory are show in figure 2B. As time progresses, motors diffuse in the surface of the cargo, motors bind and unbind from the microtubule, and cargo orientation changes as it is pulled along by forces generated by the motors, as shown in ***Figure 2–video 1***.

Cargos with free motors bind to the microtubule faster than those with rigidly anchored motors

For a cargo to be transported, one of its motors must first bind the microtubule. In this section, we use our model to investigate the time it takes for a cargo located near a microtubule to bind to it. Visualizations of example simulations for each organization mode are shown in ***Figure 3–video 1***–***Figure 3–video 4***.

We first compare the four organization modes as a function of the number of motors on the cargo, as figure 3A shows for a 0.5 μm diameter cargo. We find that for cargos in the rigid clustered mode, the mean time to bind is long when there is a single motor, and stays constant as the number of motors on the cargo increases. This can be understood by considering the timescales in the problem; cargos in this mode spend most of their time waiting until the motors are near enough to the microtubule for them to bind, as rotation is slow compared to the characteristic binding time of a single motor. A cargo in the rigid dispersed mode with only one motor is identical to a rigid clustered cargo with one motor. For rigid dispersed cargos, however, we find the time to bind decreases drastically as more motors are added. Because anchor locations are selected randomly from a uniform distribution over the surface of the cargo, the average angle though which these

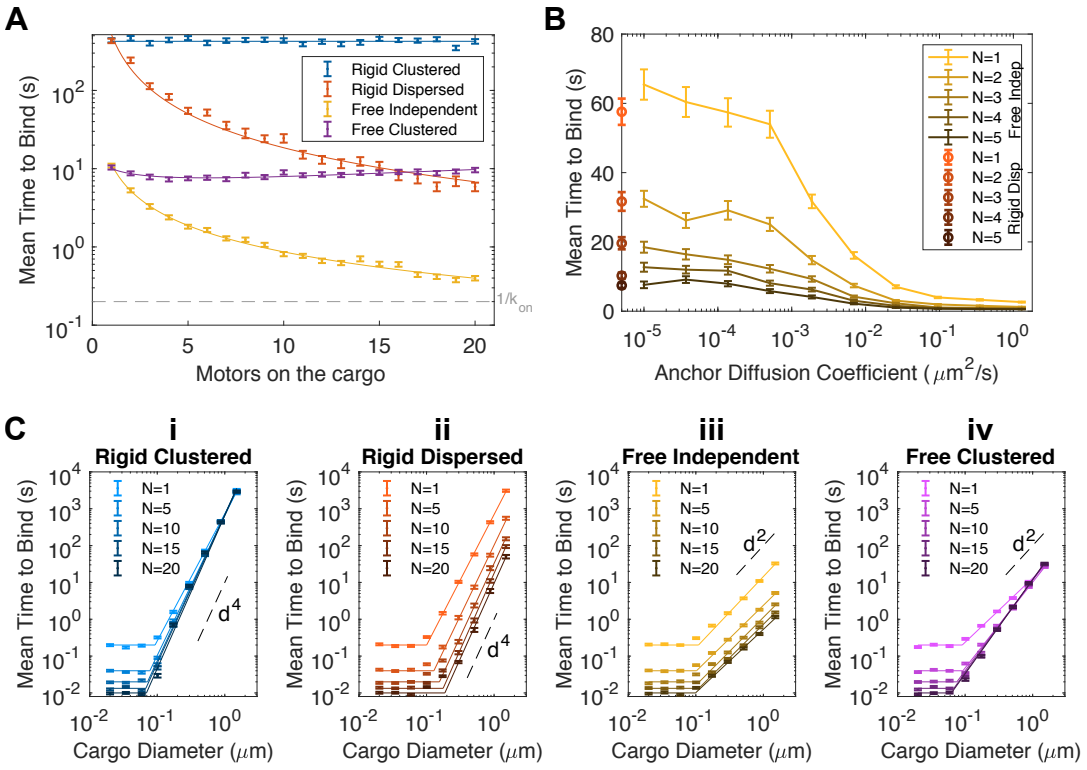

Figure 3. Times for cargos in different organization modes to bind to the microtubule
Simulated cargos are allowed to diffuse rotationally, but not translationally, with no gap between the cargo and microtubule. In all panels, error bars represent standard error of the mean of 300 simulations. Underlying distributions are approximately exponential (see figure ***Figure 3–Figure Supplement 1***).
A: Time for the cargo to bind to the microtubule for the four anchoring modes, as a function of the number of motors on the cargo. The characteristic time for a single motor to bind, assuming it is near the microtubule, is shown in dashed grey. Distributions of times to bind in the different modes are shown in figure ***Figure 3–Figure Supplement 1***A. Overlaid curves are fits, detailed in table ***Figure 3–Figure Supplement 2***.
B: Dependance of the cargo binding time on the diffusion coefficient of the motor anchors in the cargo membrane for the free independent mode. Red errorbars located on the left vertical axis are mean binding time for the rigid dispersed mode, to which the free independent mode reduces at low diffusion coefficients. Distributions of binding times at the indicated diffusion coefficients are shown in figure ***Figure 3–Figure Supplement 1***Bi. Distributions of binding times for the lowest diffusion coefficient and rigid dispersed cargos are shown together in figure***Figure 3–Figure Supplement 1***Bii. Lines between points are guides for the eye.
C: Time for the cargo to bind as a function of the cargo radius for the four anchoring modes (**i-iv**), shown for various values of the number of motors on the cargo, N. Dashed lines indicating scaling with diameter to the fourth power (**i** and **ii**) and diameter to the second power (**iii-iv**) are shown for comparison. Overlaid curves are fits, detailed in ***Figure 3–Figure Supplement 2***.

Figure 3–Figure supplement 1. Cargo time to bind distributions

Figure 3–Figure supplement 2. List fit values

Figure 3–video 1. Animation of cargo binding for cargo with rigid clustered motors

Figure 3–video 2. Animation of cargo binding for cargo with rigid dispersed motors

Figure 3–video 3. Animation of cargo binding for cargo with free independent motors

Figure 3–video 4. Animation of cargo binding for cargo with free clustered motors

cargos must rotate before a motor comes within reach of the microtubule decreases as motors are added. This change is most drastic for the first few motors, with the time to bind of these 0.5 μm diameter cargos decreasing by an order of magnitude with the addition of only 5 motors.

We find that 0.5 μm diameter cargos with a single free motor with diffusion coefficient 0.1 $\mu m^2\ s^{-1}$ bind more than an order of magnitude faster than cargos of the same size with a single rigidly attached motor. This also can be understood by considering timescales; diffusion on the surface is much faster than rotational diffusion of the cargo, so less time is spent waiting for a motor to come near the microtubule. When free motors are added in a cluster, we find that time to bind is independent of the number of motors in that cluster. This indicates that the time spent waiting for motors to come near the microtubule is the slowest process, as the increased binding rate of the motors in the cluster do not decrease the time to bind. When anchors are independent, time to bind goes down drastically as the number of motors is increased. This effect includes both the decreased time to bind from the spread out initial locations of the motors, as well as the fact that each motor performs its own search. While anchor motions are all subject to the same contribution from the rotational diffusion of the cargo, the rotation timescale is much slower than surface diffusion, making each search almost independent at this cargo size and diffusion coefficient.

The results of figure 3 indicate that at 0.1 $\mu m^2\ s^{-1}$, surface diffusion is much faster than cargo rotation. At some diffusion coefficient, surface diffusion should become slower than cargo rotation, and the time to bind for free independent cargos should approach that of rigid dispersed cargos. We find that the motor diffusion coefficient must be decreased by orders of magnitude to obtain significant changes in the time to bind, as shown in figure 3B. For the 0.5 μm diameter cargos shown, diffusion coefficient of the motors must be lower than $10^{-4}\ \mu m^2\ s^{-1}$ for free independent cargos to have times to bind similar to rigid dispersed cargos.

We find that times to bind for cargos in each of the organization modes depend differently on the cargo size. When cargos are small enough that all motors can simultaneously reach the microtubule (∼50 nm diameter), the time to bind for cargos in all organization modes is the same. As cargo size increases, time to bind remains dependent only on motor number until cargos reach ∼100 nm in diameter. For cargos larger than this, scaling of time to bind with size is drastically different for cargos in the different organization modes. For cargos with rigidly attached motors, time to bind scales with approximately the fourth power of the cargo diameter. For cargos in the free independent mode, time to bind scales with only (roughly) the second power of the diameter. Free clustered cargos with one motor are identical to free independent cargos with one motor, and therefore must have the same scaling. As the number of motors increases, however, scaling becomes more severe, nearing the scaling of rigid motors at high motor number.

Cargos with free independent motors form dynamic clusters which increase travel distance

We next investigate the distance that cargos travel, after initial attachment to the microtubule. To do so, we begin simulations with a single motor bound to the microtubule and simulate until the cargo reaches a state in which all motors are detached from the microtubule. A few stochastic trajectories, along with the mean position over many cargos are shown as a function of time in figure 4A (top). Once bound to the microtubule, rigid clustered cargos and free clustered cargos behave similarly. Hereafter, we show only results for rigid clustered cargos and refer to them as "clustered" to reflect this. Visualizations of example simulations for each organization mode are shown in ***Figure 4–video 1–Figure 4–video 3***.

We find that cargo run lengths depend strongly on motor organization mode. For cargos with clustered motors, just four motors working together give run lengths on the order of the size of a cell. Motors in this mode work together very well, as if any motor is bound the rest of the motors are located where they are also able to bind the microtubule. This contrasts with the dispersed mode, where many motors are necessary to achieve run lengths of a few microns. For the 0.5 μm diameter cargos plotted in figure 4B, 25 motors are required to achieve a mean run length of 3 μm.

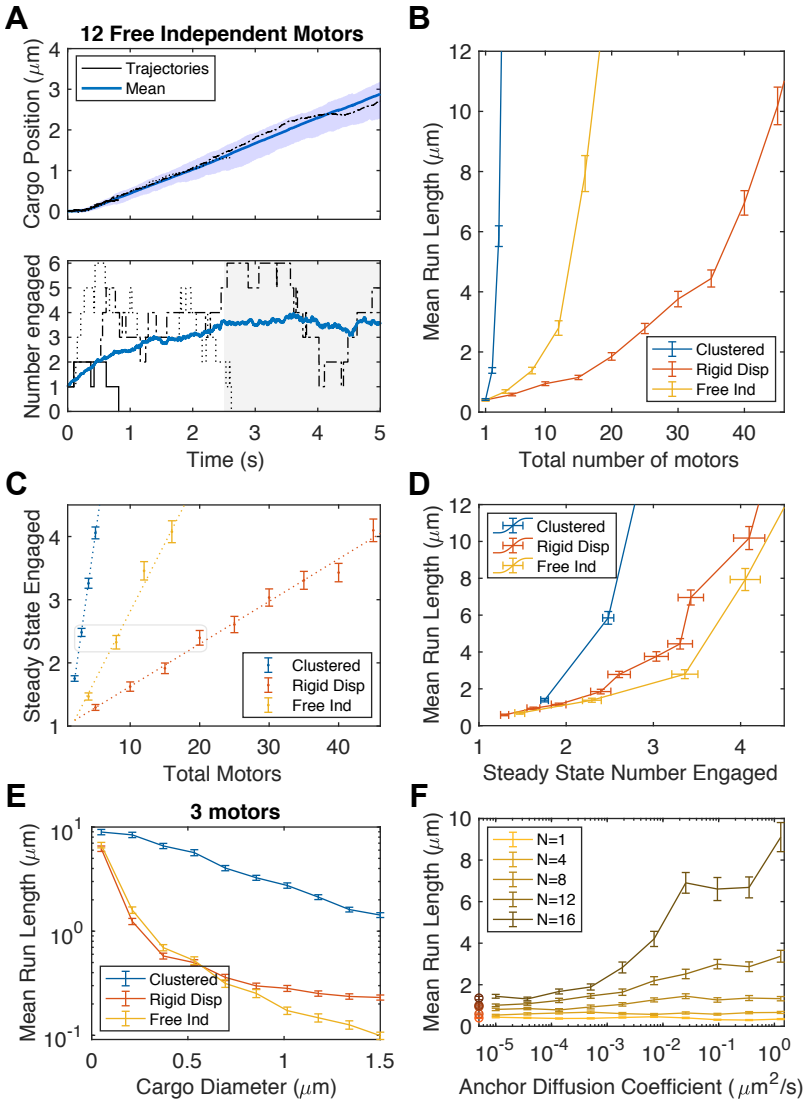

Figure 4. Free independent cargos have longer run lengths than rigid dispersed cargos due to dynamic clustering. **A**: Position (top) and number of motors engaged (bottom) with time for free independent cargos with 12 total motors. Trajectories of three cargos are shown in black and the mean over 100 cargos is shown in dark blue. Cargos are excluded from the calculation after they fall off the microtubule. The area between the 5th and 95th percentile positions is shaded in blue in the top panel. Times greater than the time to steady state are shaded in grey in the bottom panel. **B**: Mean run lengths for cargos in each of the three anchor modes as a function of the total number of motors on the cargo. Distributions of run lengths are shown in figure ***Figure 4–Figure Supplement 1***A. **C**: Mean number of motors engaged at steady state versus motor number for the 3 anchor modes. Linear fits are shown as dotted lines. For values, see ***Figure 4–Figure Supplement 2***. Grey box indicates conditions with similar mean number engaged at steady state which will be compared in later figures. **D**: Mean run length as a function of steady state number of engaged motors for the three anchoring modes. **E**: Mean run length for cargos with three total motors as a function of cargo size for each of the three anchoring modes. **F**: Mean run length for cargos with free independent motors as a function of the diffusion coefficient of the motors in the cargo membrane, for different numbers of total motors. Red errorbars overlaid on the left axis are for rigid dispersed cargos of the same total numbers. In **B**, **E** and **F**, error bars are SEM of 300 cargos. In **C**, error bars are SEM of 100 cargos. In **B**, **D**, **E** and **F** lines between points are guides for the eye.

Figure 4–Figure supplement 1. Run Length Distributions

Figure 4–Figure supplement 2. List fit values

Figure 4–video 1. Animation of run length for cargo with rigid clustered motors

Figure 4–video 2. Animation of run length for cargo with rigid dispersed motors

Figure 4–video 3. Animation of run length for cargo with free independent motors

These results are consistent with previous work comparing these two modes (***Erickson et al., 2011***).

For cargos with free independent motors, we find run lengths which are longer than those of dispersed cargos, but not as long as those of clustered cargos. One possibility is that the run lengths are due to the number of motors which are instantaneously bound to the microtubule at a given time, which we term the number engaged. We therefore query this quantity in our simulations. The number of motors engaged on the microtubule fluctuates with time. Several stochastic trajectories are shown in figure 4A (bottom), along with the mean over 100 cargos at each time. We find that the mean number of motors engaged rises from the initial condition of 1 to a steady state value over a period of time. In figure 4C, we show that free independent cargos have more motors engaged than rigid dispersed cargos. The initial locations of motors on the surface of cargos in these two modes is the same, i.e., uniformly random on the surface. Therefore, the increased steady state number of engaged motors on free independent cargos indicates that motors are diffusing to the microtubule, binding, and remaining bound for longer than they would if simply placed randomly. In other words, the motors cluster near the microtubule. These clusters are dynamic, with motors diffusing in and binding, as well as unbinding and diffusing away, as can be seen in ***Figure 2–video 1*** and **??**freeindependent.

How strong is the clustering effect? In the range of total motor numbers investigated, the number of engaged motors is 25 % to 30 % of the total number on the cargo. This is more than the 10 % to 15 % of motors engaged on rigid dispersed cargos, but less than the $\sim$ 80 % of motors engaged on clustered cargos (figure 4C). So, while dynamic clusters contain more motors than would available to bind the microtubule if motors were distributed randomly on the surface, they do not contain all or even most of the motors on the cargo.

We hypothesized that dynamic clustering is responsible for free independent cargos' enhanced run length over rigid dispersed cargos. To test this hypothesis, we plot mean run length vs. steady state number engaged. If dynamic clustering is responsible for the enhanced run length, we expect the free independent and rigid clustered modes to have the same run length once the greater number of engaged motors is corrected for. We see in figure 4D that data from the two modes is similar. Run lengths for free independent cargos are in fact slightly lower once corrected for number of engaged motors. This is surprising because cargos with similar mean numbers of motors engaged at steady state have similar distributions of motors engaged, as shown in ***Figure 4–Figure Supplement 1***B. In ***Figure 4–Figure Supplement 1***C, we show that the lower run length is explained by a longer time to steady state and resultantly more cargos which fall off the microtubule at early times.

The three modes also differ significantly in their dependance on cargo size. In figure 4E, we show that cargos with clustered motors have a run length that depends only weakly on cargo size, while free independent and rigid dispersed cargos have a more complex dependance.

The run length advantage of free independent cargos over rigid dispersed ones should, like the binding time advantage, be reduced to zero at low anchor diffusion coefficients. In figure 4F, we show that the diffusion coefficient must be reduced by orders of magnitude to have significant impacts on run length. We find that diffusion coefficients below 10^{-4} μm^2 s^{-1} are effectively rigid, which is a similar to the threshold we found for time-to-bind.

Cargos with free independent motors are better able to transport against a load compared to cargos with rigid dispersed motors

A cargo's ability to generate a sustained force is also important for navigating the crowded environment of the cell. In this section, we examine the run lengths of cargos in the different organization modes against a constant force.

As expected, we find that that increasing force decreases the run length of cargos, no matter what the organization mode or number of motors, as can be seen in ***Figure 5–Figure Supplement 1***A. We find that 7 pN of force is sufficient to reduce the run lengths from 20 μm or more to nearly zero in every organization mode.

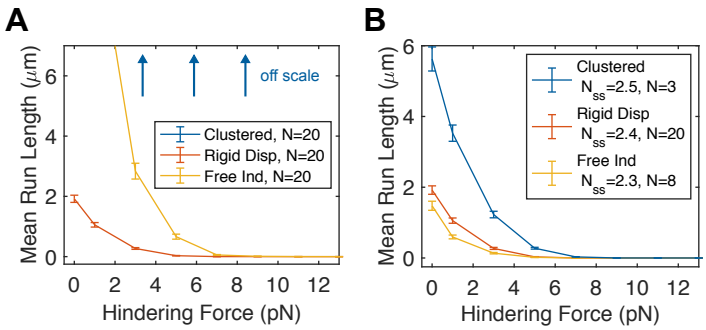

Figure 5. Cargos with free independent motors travel farther under load due to dynamic clustering.
Mean run lengths as a function of external hindering load on the cargo for cargos in each of the three modes, with
A: matched total number of motors. Cargos with 20 clustered motors travel farther than 20 μm on average, and are not shown to clarify the difference between rigid dispersed and free independent modes.
B: matched number of motors engaged at steady state (at 0 external load). Distributions of run lengths for these cargos can be found in ***Figure 5–Figure Supplement 1***C.
Error bars are standard error of the mean over 300 cargos in both **A** and **B**. Lines between points are guides for the eye.

Figure 5–Figure supplement 1. Forces on cargo

We now compare the run length of cargos in different organization modes under force. In figure 5A, we show that cargos with 20 free independent motors have significantly longer run lengths than cargos with the same number of rigid dispersed motors, when subject to forces up to 7 pN. At higher forces, run lengths for these cargos are effectively zero. At this high number of motors, cargos with clustered motors travel long distances, even when loaded with 12 pN or more (figure 5A, arrows). When the number of total motors is 5, we can see that cargos with clustered motors outperform both rigid dispersed and free independent cargos (***Figure 5–Figure Supplement 1***B). At this low number of total motors, cargos in rigid dispersed and free independent modes are almost always driven by a single motor, so differences between the two modes are not apparent.

Are enhanced run lengths under force also solely due to changes in the number engaged? To test this hypothesis, we plot run lengths under force for cargos in the three organization modes with total numbers of motors which give the cargos matching steady state numbers of engaged motors (at 0 force, indicated by box in figure 4C). Like in the zero force case, we find that cargos with free independent motors have similar, but slightly lower run lengths than cargos with dispersed motors when compared with the same steady state number engaged. Therefore, the enhanced run length of free independent motors under load comes from the ability of motors to form dynamic clusters, like in the unloaded case. A priori, for an equal number of engaged motors, we expected differences between a dynamic cluster and static arrangements in the way the load is shared among these engaged motors, with dynamic clusters better able to share the load. However, we do not find this effect is strong enough to outperform cargos with rigid dispersed motors on a per-motor-engaged basis.

Discussion

While transport of subcellular cargo by molecular motors is increasingly understood, the extension of this understanding to control of cell internal organization will involve studying the three-way interplay between the cargo, the MT and local environment, and the motors. In this work, we developed a computational model of the motors' interaction with the cargo, assuming different modes of organization: both position and its freedom to change via membrane fluidity. We found that cargos with rigidly attached motors face a tradeoff between, on the one hand, time for the cargo to bind to a nearby microtubule and, on the other, the run length of cargos after bound. Rigid clustered motors bind slowly, but have long run lengths. Rigid dispersed cargos bind faster than

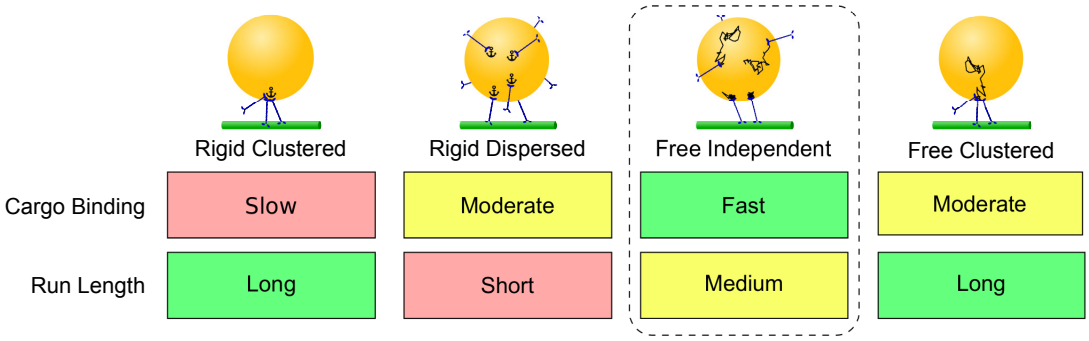

Figure 6. We find that different organizations of the motors on the cargo have different implications for how rapidly the cargo will bind to a nearby microtubule and the cargo's ability to travel along the microtubule. For cargos with motors rigidly bound, (first two columns) there is a tradeoff between clustered motors, which are slow to bind the microtubule, but travel long distances, and dispersed motors, which bind the microtubule quickly but are have poor travel distances. Cargos with freely diffusing motors (third column), at reasonable surface diffusion coefficients, cargo sizes and motor numbers, overcome this tradeoff. They bind the microtubule at least as fast as rigidly dispersed motors, and faster for large and realistic estimates of diffusion coefficient. They travel farther than rigid dispersed motors because of the formation of dynamic clusters. Because these clusters have high internal turnover, travel distances are lower than that of a rigid cluster. For a cargo with a freely diffusing cluster of motors (fourth column), cargo binding may behave more like a rigid cluster or freely diffusing motors, depending on parameters. Once it has bound the microtubule, it behaves indistinguishably from a rigid cluster in both run length and force generation.

rigid clustered cargos, but have short run lengths. Our main result is that, depending on parameters, cargos with free motors can overcome this tradeoff (figure 6). Cargos with free independent motors bind faster than cargos in either of the rigid modes, and have run lengths which are longer than those of rigid dispersed cargos, but not as long as clustered cargos. When motors are arranged in a free cluster, cargos have the same long run lengths as rigid clusters, as well as binding to a nearby microtubule more quickly. The time to bind is not as fast a free independent cargo, however, or even a rigid dispersed cargo with many motors.

This work adds to a growing body of evidence that, first, the position of motors on the cargo (whether free or not) impacts transport (***Erickson et al., 2011***; ***Sanghavi et al., 2018***); second, that mobility on the cargo surface further influences transport (***Li et al., 2018***; ***Chowdary et al., 2018***; ***Grover et al., 2016***; ***Lombardo et al., 2017***; ***Lüdecke et al., 2018***); and, third, that there are significant differences in the arrangement of motors on cargo in cells (***Rai et al., 2016***; ***Chowdary et al., 2018***), for example via changes to lipid content (***Neefjes et al., 2017***; ***Pathak and Mallik, 2017***). The closest direct experimental study related to our work is by ***Li et al.*** (***2018***). This work was in vitro, where the viscosity is orders of magnitude smaller. They find broad agreement with our simulations that fluid membranes enhance transport. However, the details are different: The velocity changes are weak and run-lengths changes are undetectable. Our work thus highlights an important role for the rheological properties of the cytoplasm, and the difficulty extrapolating in vitro results into the cellular environment.

We find that time to bind and run length are sensitive to cargo size in different ways for the four organization modes. Rigid dispersed cargos have a time to bind which scales up strongly as cargo size increases, but run length is relatively insensitive to cargo size. The time to bind for rigid dispersed cargos also scales strongly, but their run length is more sensitive to cargo size in comparison to rigid clustered cargos. Free independent cargos have a much weaker scaling of time to bind, as well as an intermediate dependance of run length on cargo size. These different scalings raise the possibility that the cell could use the size dependent behaviors to differentially direct otherwise similar cargos.

Moreover, the differences in scaling law exponents we uncover are independent of model details, e.g., motor parameters and molecular numbers. Therefore, binding time scaling could be used to

identify the organization of motors on cargos from the cell. Using the natural variability of cargo sizes to uncover different scaling exponents could inform whether the motors are free or not.

Our work is in broad agreement with (***Chowdary et al., 2018***), who combined advanced microscopy and tracking with a computational model to give insight into the motion of endosomes in axons. They report the emergence of dynamic clustering in their simulation via preference for binding the MT track. Their simulation allows motors to move on the surface of a cargo independent of each other and of rotations of the cargo itself. Our work extends this by considering a model in which motor anchor position, cargo rotation and cargo translation are all coupled with both cytoplasmic viscosity/fluctuations and membrane viscosity/fluctuations, via a force-balance relationship at every time point. Particularly interesting complexity arises, e.g., the two viscosities give rise to fluctuations that are, in the lab frame of reference, no longer uncorrelated (see supplemental). Doing so allowed us to explore a wide range of parameters, from the limit in which the cargo membrane is inviscid and the motor can step along the MT without moving the cargo, all the way to a static anchoring. It also allowed us to explore the competition between cargo rotation and diffusion of motors to drive binding time – of particular importance when the cargos are small. The coupling via force-balance also led to an emergent inter-motor communication via how each motor is loaded, which influenced predicted run lengths. Interestingly, we find that dynamic clustering is not a strong effect for all parameters regimes. For example, at physiological parameters, we find only 25% of the motors are clustered (e.g., figure 4).

That the transport machinery is sensitive to motor organization opens several possible directions of future work. First, cargos in the cell exist in a microtubule network with a specific architecture (***Ando et al., 2015***; ***Ciocanel et al., 2018***; ***Bergman et al., 2018***; ***Erickson et al., 2013***). The current work focused on exploring interaction with a single MT, but could readily be extended. Second, many cargos are deformable (***Driller-Colangelo et al., 2016***) and this might lead to significant differences in transport. While deformability of a large cargo will lead to transport changed by interacting with the environment, e.g., spacing of nearby cytoskeletal elements and organelles, our work suggests cargo deformability might also impact transport more directly via changes to motor organization. Finally, motors are sensitive to MT-associated proteins (MAPs) (***Dixit et al., 2008***; ***Vershinin et al., 2007***). The accessibility of the motors to MAPs is expected to exhibit similar behavior to the accessibility of motors to the MT, which we have shown varies widely depending on organization mode.

Acknowledgments

This work was supported by NIH R01 GM123068 to JA and SG, NIH T32 Training Grant EB009418-07 to Arthur Lander and Qing Nie, the UCI Center for Complex Biological Systems, the BEST IGERT program funded by the National Science Foundation DGE-1144901, NSF grant DMS 1763272 and a grant from the Simons Foundation (594598, QN).

References

Ahmed, W. W., Fodor, É., Almonacid, M., Bussonnier, M., Verlhac, M. H., Gov, N., Visco, P., van Wijland, F., and Betz, T. (2018). Active Mechanics Reveal Molecular-Scale Force Kinetics in Living Oocytes. *Biophysical Journal*, 114(7):1667–1679.

Akhmanova, A. and Hammer, J. A. (2010). Linking molecular motors to membrane cargo. *Curr Opin Cell Biol.* 22(4): 479–487.

Ando, D., Korabel, N., Huang, K. C., and Gopinathan, A. (2015). Cytoskeletal Network Morphology Regulates Intracellular Transport Dynamics. *Biophysical Journal*, 109(8):1574–1582.

Andreasson, J. O., Milic, B., Chen, G. Y., Guydosh, N. R., Hancock, W. O., and Block, S. M. (2015). Examining kinesin processivity within a general gating framework. *eLife*, 2015(4):1–44.

Bergman, J. P., Bovyn, M. J., Doval, F. F., Sharma, A., Gudheti, M. V., Gross, S. P., Allard, J. F., and Vershinin, M. D. (2018). Cargo navigation across 3D microtubule intersections. *Proceedings of the National Academy of Sciences of the United States of America*, 115(3):537–542.

Chowdary, P. D., Kaplan, L., Che, D. L., and Cui, B. (2018). Dynamic Clustering of Dyneins on Axonal Endosomes: Evidence from High-Speed Darkfield Imaging. *Biophysical Journal*, 115(2):230–241.

Ciocanel, M.-V., Sandstede, B., Jeschonek, S. P., and Mowry, K. L. (2018). Modeling Microtubule-Based Transport and Anchoring of mRNA. *SIAM Journal on Applied Dynamical Systems*.

Dixit, R., Ross, J. L., Goldman, Y. E., and Holzbaur, E. L. F. (2008). Differential Regulation of Dynein and Kinesin Motor Proteins by Tau. *Science*, 319(5866):1086 LP – 1089.

Driller-Colangelo, A. R., Chau, K. W., Morgan, J. M., and Derr, N. D. (2016). Cargo rigidity affects the sensitivity of dynein ensembles to individual motor pausing. *Cytoskeleton*, 73(12):693–702.

Erickson, R. P., Gross, S. P., and Yu, C. C. (2013). Filament-Filament Switching Can Be Regulated by Separation Between Filaments Together with Cargo Motor Number. *PLoS ONE*, 8(2):e54298.

Erickson, R. P., Jia, Z., Gross, S. P., and Yu, C. C. (2011). How Molecular Motors Are Arranged on a Cargo Is Important for Vesicular Transport. *PLoS Computational Biology*, 7(5):e1002032.

Feng, Q., Mickolajczyk, K. J., Chen, G. Y., and Hancock, W. O. (2018). Motor Reattachment Kinetics Play a Dominant Role in Multimotor-Driven Cargo Transport. *Biophysical Journal*, 114(2):400–409.

Grover, R., Fischer, J., Schwarz, F. W., Walter, W. J., Schwille, P., and Diez, S. (2016). Transport efficiency of membrane-anchored kinesin-1 motors depends on motor density and diffusivity. *Proceedings of the National Academy of Sciences of the United States of America*, 113(46):E7185–E7193.

Guo, M., Ehrlicher, A. J., Jensen, M. H., Renz, M., Moore, J. R., Goldman, R. D., Lippincott-Schwartz, J., Mackintosh, F. C., and Weitz, D. A. (2014). Probing the stochastic, motor-driven properties of the cytoplasm using force spectrum microscopy. *Cell*, 158(4):822–832.

Herms, A., Bosch, M., Reddy, B. J., Schieber, N. L., Fajardo, A., Rupérez, C., Fernández-Vidal, A., Ferguson, C., Rentero, C., Tebar, F., Enrich, C., Parton, R. G., Gross, S. P., and Pol, A. (2015). AMPK activation promotes lipid droplet dispersion on detyrosinated microtubules to increase mitochondrial fatty acid oxidation. *Nature Communications*, 6:7176.

Keller, S., Berghoff, K., and Kress, H. (2017). Phagosomal transport depends strongly on phagosome size. *Scientific Reports*, 7(1):1–15.

Klumpp, S. and Lipowsky, R. (2005). Cooperative cargo transport by several molecular motors. *Proc Natl Acad Sci USA*, 102(48):17284–9.

Kunwar, A., Vershinin, M., Xu, J., and Gross, S. P. (2008). Stepping, Strain Gating, and an Unexpected Force-Velocity Curve for Multiple-Motor-Based Transport. *Current Biology*, 18(16):1173–1183.

Kusumi, A., Tsunoyama, T. A., Hirosawa, K. M., Kasai, R. S., and Fujiwara, T. K. (2014). Tracking single molecules at work in living cells. *Nature Chemical Biology*, 10(7):524–532.

Li, Q., Tseng, K.-F., King, S. J., Qiu, W., and Xu, J. (2018). A fluid membrane enhances the velocity of cargo transport by small teams of kinesin-1. *Journal of Chemical Physics*, 148(12):123318.

Lombardo, A. T., Nelson, S. R., Ali, M. Y., Kennedy, G. G., Trybus, K. M., Walcott, S., and Warshaw, D. M. (2017). Myosin Va molecular motors manoeuvre liposome cargo through suspended actin filament intersections in vitro. *Nature Communications*, 8:15692.

Lüdecke, A., Seidel, A. M., Braun, M., Lansky, Z., and Diez, S. (2018). Diffusive tail anchorage determines velocity and force produced by kinesin-14 between crosslinked microtubules. *Nature Communications*, 9:2214.

Maday, S., Twelvetrees, A. E., Moughamian, A. J., and Holzbaur, E. L. F. (2014). Axonal transport: cargo-specific mechanisms of motility and regulation. *Neuron*, 84(2):292–309.

Milo, R., Jorgensen, P., Moran, U., Weber, G., and Springer, M. (2010). BioNumbers, the database of key numbers in molecular and cell biology. *Nucleic Acids Research*, 38(SUPPL.1):750–753.

Neefjes, J., Jongsma, M. M., and Berlin, I. (2017). Stop or Go? Endosome Positioning in the Establishment of Compartment Architecture, Dynamics, and Function. *Trends in Cell Biology*, 27(8):580–594.

Pathak, D. and Mallik, R. (2017). Lipid - Motor Interactions: Soap Opera or Symphony? *Current Opinion in Cell Biology*, 44:79–85.

Rai, A., Pathak, D., Thakur, S., Singh, S., Dubey, A. K., and Mallik, R. (2016). Dynein Clusters into Lipid Microdomains on Phagosomes to Drive Rapid Transport toward Lysosomes. *Cell*, 164(4):722–734.

Saffman, P. G. and Delbrück, M. (1975). Brownian motion in biological membranes. *Proceedings of the National Academy of Sciences of the United States of America*, 72(8):3111–3.

Sanghavi, P., D'Souza, A., Rai, A., Rai, A., Padinhatheeri, R., and Mallik, R. (2018). Coin Tossing Explains the Activity of Opposing Microtubule Motors on Phagosomes. *Current Biology*, 28(9):1460–1466.e4.

Shubeita, G. T., Tran, S. L., Xu, J., Vershinin, M., Cermelli, S., Cotton, S. L., Welte, M. A., and Gross, S. P. (2008). Consequences of Motor Copy Number on the Intracellular Transport of Kinesin-1-Driven Lipid Droplets. *Cell*, 135(6):1098–1107.

Sigurdsson, J. K. and Atzberger, P. J. (2016). Hydrodynamic coupling of particle inclusions embedded in curved lipid bilayer membranes. *Soft Matter*, 12(32):6685–6707.

Sumi, T. (2017). Design principles governing chemomechanical coupling of kinesin. *Scientific Reports*, 7(1):1163.

Verhey, K. J., Kaul, N., and Soppina, V. (2011). Kinesin Assembly and Movement in Cells. *Annual Review of Biophysics*, 40(1):267–288.

Vershinin, M., Carter, B. C., Razafsky, D. S., King, S. J., and Gross, S. P. (2007). Multiple-motor based transport and its regulation by Tau. *Proc Natl Acad Sci USA*, 104(1):87–92.

Wilhelm, C., Gazeau, F., and Bacri, J. C. (2003). Rotational magnetic endosome microrheology: Viscoelastic architecture inside living cells. *Physical Review E*, 67(6):12.

Xu, J., Shu, Z., King, S. J., and Gross, S. P. (2012). Tuning Multiple Motor Travel via Single Motor Velocity. *Traffic*, 13(9):1198–1205.

Yamada, S., Wirtz, D., and Kuo, S. C. (2000). Mechanics of living cells measured by laser tracking microrheology. *Biophysical Journal*, 78(4):1736–1747.

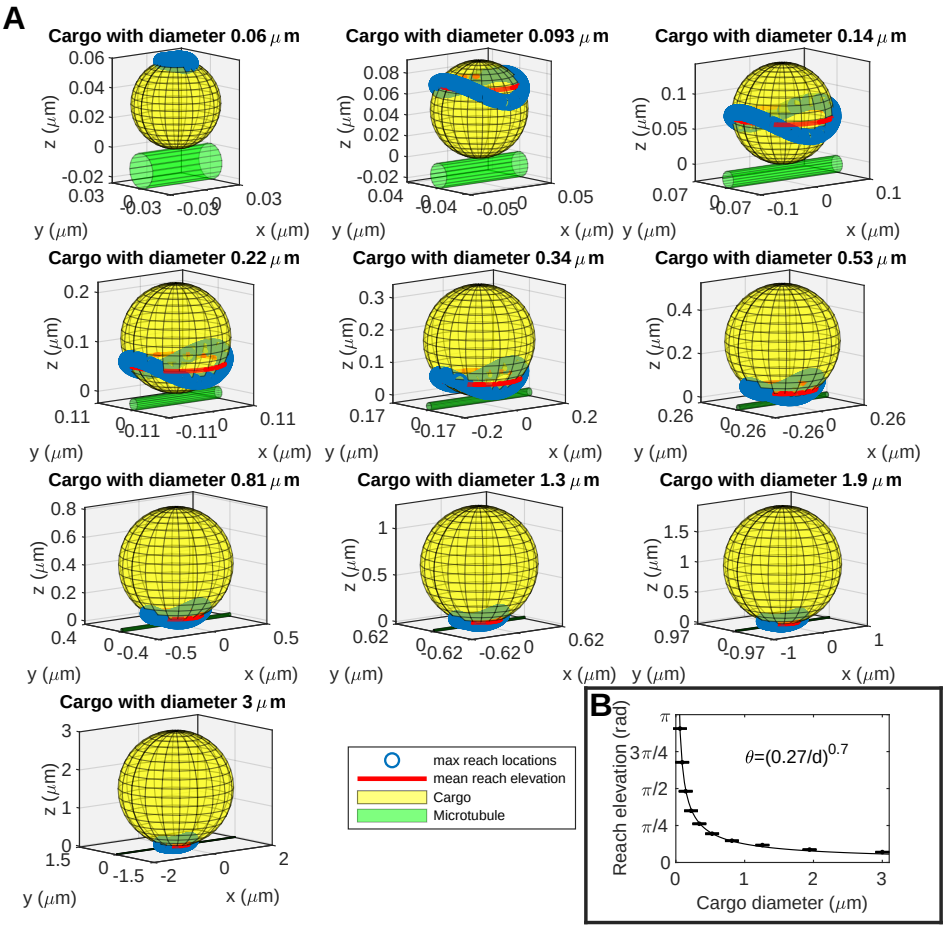

458

Figure 1–Figure supplement 1. Mean reach elevation and calculation of mean first passage time to the microtubule. In figure 1 we show an estimate of the time it would take for a motor, initially opposite the microtubule, to come within reach of it. These times come from analytical expressions for mean first passage time to a spherical cap, $\frac{8\pi\eta R^3}{k_B T}\log\left(\frac{1-\cos(\pi)}{1-\cos(\theta)}\right)$ for rotational diffusion of the cargo and $\frac{R^2}{D}\log\left(\frac{1-\cos(\pi)}{1-\cos(\theta)}\right)$ for diffusion in the cargo surface. Here η represents viscosity (of the fluid surrounding the cargo), R is the cargo radius, k_B is Boltzmann's constant, T is temperature, and D is diffusion coefficient (of the motor in the cargo surface). To apply these equations, we had to first estimate θ, the extent of the spherical cap to which the motor must diffuse before binding. To do so, we simulated motors diffusing from the north pole of the cargo and recorded the first anchor location where the motor was able to bind with its maximum rate as described in supplemental section A.3.3, referred to as a max reach location. We then used the mean elevation of these points as our estimate for θ. Cargo and microtubule were situated as shown in **A**. For details on how we model the mechanics of a motor and it's attachment to the cargo, see supplemental section A.1.1. **A**: Mean reach elevation for cargos of various sizes, as labeled in each panel. Legend in final panel applies to every other panel. **B**: Mean reach elevation for each cargo size shown in **A**. Bars represent standard error of the mean. Data are well fit to reach elevation $\theta = (.27/d)^{.7}$, where d is cargo diameter (black curve).

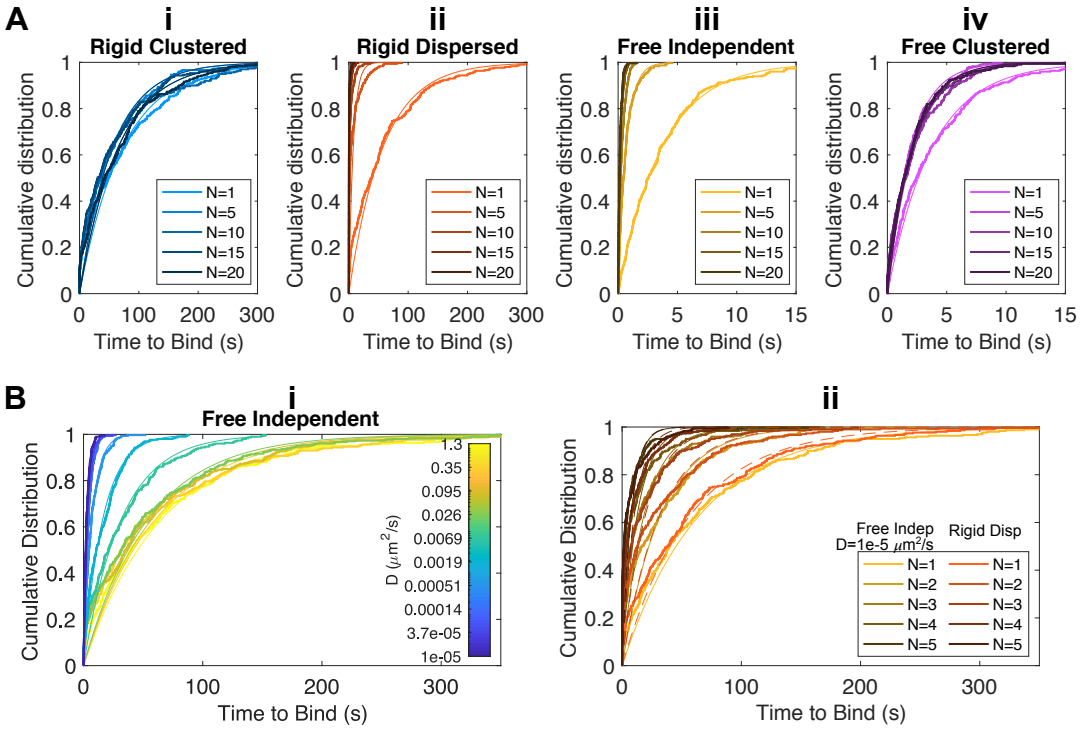

Figure 3–Figure supplement 1. Distributions of times for cargos to bind to the microtubule. **A**i-iv: Empirical cumulative distributions of time to bind for cargos in each of the four organization modes. Thinner curves of the same color are exponential fits to the data. **B**i: Empirical cumulative distributions for free independent cargos with a range of motor diffusion coefficients D. Diffusion coefficients are log spaced, values of D for each distribution shown are labeled on the colorbar. Thinner curves of the same color are exponential fits to the data. **B**ii: Empirical cumulative distributions of times to bind for free independent cargos at diffusion coefficient $D = 1 \times 10^{-5}$ μm^2 s^{-1} for several numbers of motors on the cargo (yellows). Also shown are distributions for rigid dispersed cargos at the same numbers of total motors (reds). Thinner curves of the same color are exponential fits to the data. Dashed curves are fits for rigid dispersed cargos.

Figure	Data	Equation	Values	95 % CI	Notes
3A	Rigid Clustered	aN^0	a: 424.5	410, 439	
	Rigid Dispersed	$(a/N)^b$	a: 75.37	63.94, 86.8	
			b: 1.445	1.366, 1.524	
	Free Independent	$(a/N)^b$	a: 8.777	8.49, 9.063	
			b: 1.119	1.075, 1.162	
	Free Clustered	$(a/N)^b + cN$	a: 4462	-5173, 1.41e+04	
			b: 0.2713	0.1942, 0.3484	
			c: 0.2708	0.218, 0.3237	
3Ci	$N = 1$	ad^b	b: 3.449	3.278, 3.619	Fit to d >0.03 µm
	$N = 5$		b: 3.798	3.574, 4.022	
	$N = 10$		b: 3.971	3.69, 4.253	
	$N = 15$		b: 4.033	3.733, 4.334	
	$N = 20$		b: 4.153	3.663, 4.644	
3Cii	$N = 1$	ad^b	b: 3.547	3.136, 3.959	Fit to d >0.1 µm
	$N = 5$		b: 3.826	3.224, 4.428	
	$N = 10$		b: 3.973	3.47, 4.476	
	$N = 15$		b: 4.138	3.724, 4.552	
	$N = 20$		b: 4.082	3.714, 4.45	
3Ciii	$N = 1$	ad^b	b: 1.936	1.698, 2.173	Fit to d >0.1 µm
	$N = 5$		b: 1.795	1.604, 1.985	
	$N = 10$		b: 1.844	1.54, 2.148	
	$N = 15$		b: 1.816	1.51, 2.123	
	$N = 20$		b: 1.717	1.423, 2.012	
3Civ	$N = 1$	ad^b	b: 1.739	1.538, 1.941	Fit to d >0.1 µm
	$N = 5$		b: 2.327	1.992, 2.662	
	$N = 10$		b: 2.461	2.197, 2.725	
	$N = 15$		b: 2.525	2.355, 2.696	
	$N = 20$		b: 2.561	2.243, 2.88	

Figure 3–Figure supplement 2. List of fit values Fits for figure 3 done with fit function in MATLAB R2018b. Power law fits are shown in figure 3C only when the fit time is greater than $N\pi_0^{\text{micro}}$, otherwise $N\pi_0^{\text{micro}}$ (the on rate of N motors when they are all near the microtubule) is shown. Values of a are not listed for the sake of brevity.

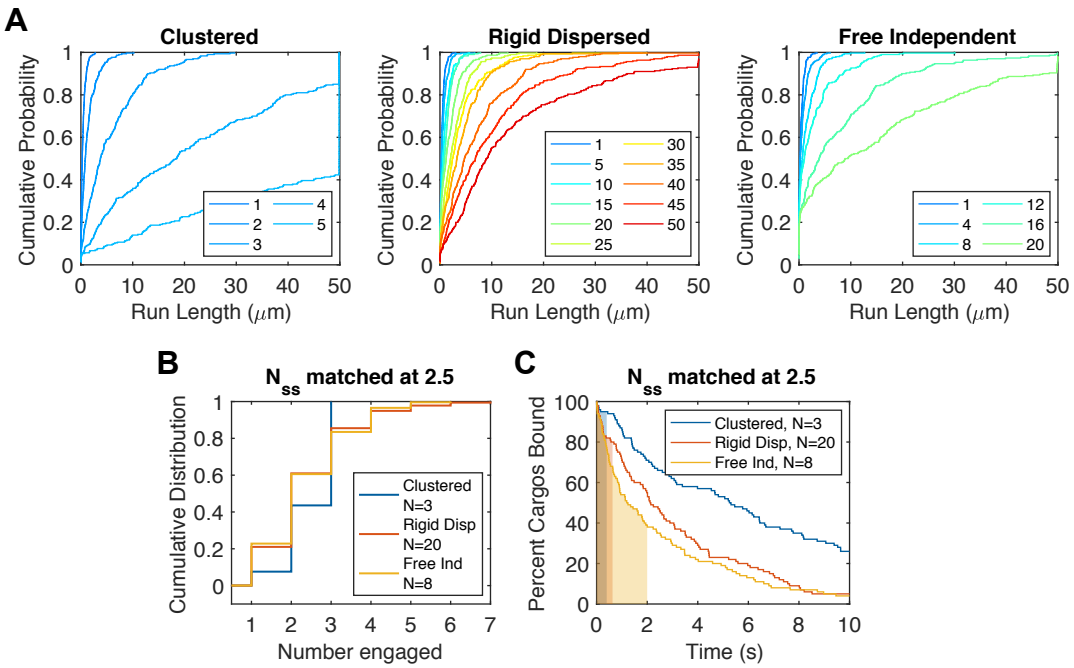

Figure 4–Figure supplement 1. Distributions of run lengths. **A**: Empirical cumulative probability distribution of run lengths for cargos in the clustered, rigid dispersed and free independent modes. Different total numbers of motors are shown on a common color axis. **B**: Empirical cumulative probability distributions of cargos with closely matched mean numbers of motors engaged at steady state (N_{ss}). Total numbers of motors N was picked for each mode to match an N_{ss} of 2.5. **C**: Percent of cargos bound as a function of time for cargos with the same total numbers of total motors N as in **B**, picked to match mean number of motors engaged at steady state, N_{ss}. The time before steady state is reached is filled in color below the curve for each organization mode.

Figure	Data	Equation	Values	95 % CI	Notes
4C	Clustered	$a + bN$	a: 0.1954		
			b: 0.7693		Get 3 more motors engaged if add 4
	Rigid Dispersed	$a + bN$	a: 0.9553		
			b: 0.0673		Need to add 15 motors to get one more engaged
	Free Independent	$a + bN$	a: 0.6585		
			b: 0.2157		Need to add 5 motors to get one more engaged

Figure 4–Figure supplement 2. List of fit values Linear fits for figure 4C done by linear regression.

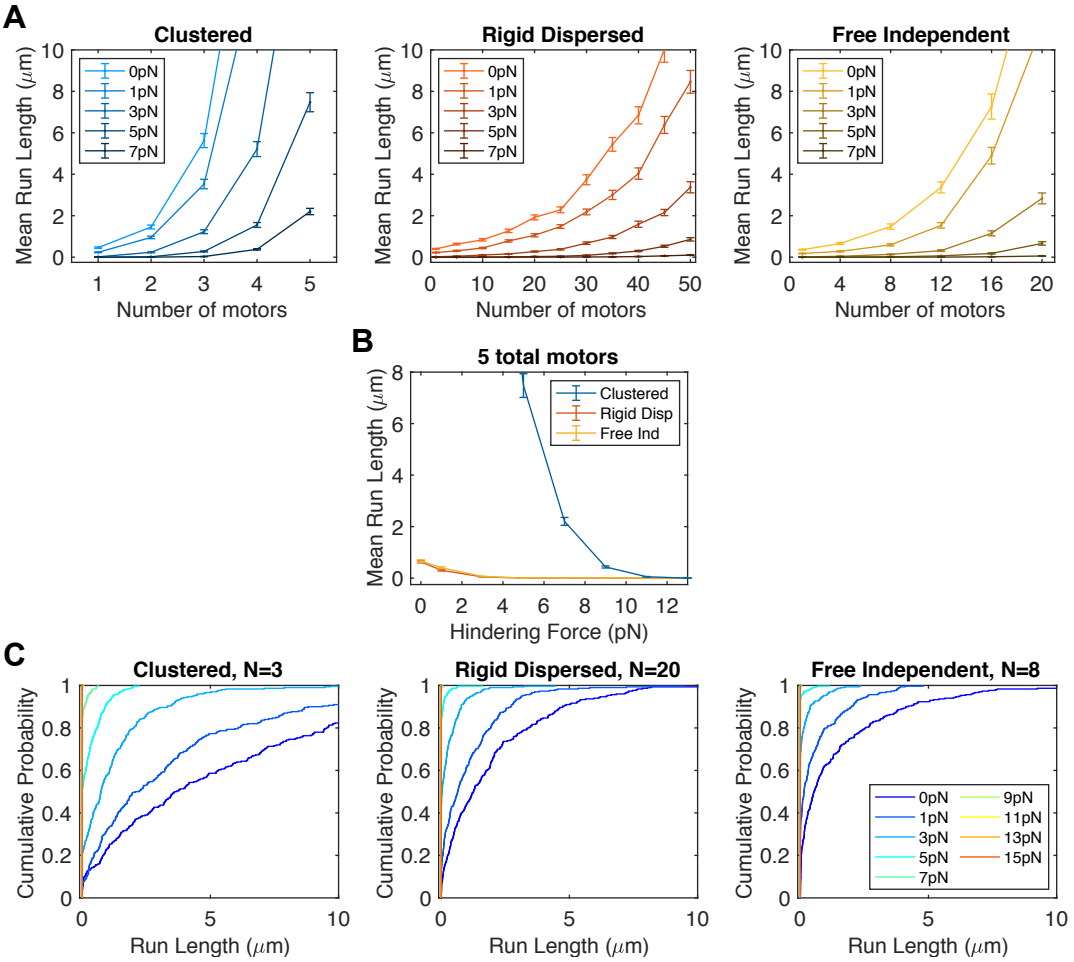

Figure 5–Figure supplement 1. Means and Distributions of run lengths under force. **A**: Run lengths as a function of the number of total numbers on the cargo for several values of hindering force on the cargo. Errorbars are standard error of the mean. **B**: Mean run lengths as a function of external hindering load on the cargo for cargos in each of the three modes, with the total number of motors on the cargo matched at 4. **C**: Distributions of run lengths of cargos under different loads. Numbers of motors are chosen to match figure 5B. Distributions are colored on a common axis corresponding to the legend in the right (free independent) panel.